Construction and performance analysis of local DtN absorbing boundary conditions for exterior Helmholtz problems. Part II : Prolate spheroid boundaries

Hélène Barucq, Rabia Djellouli, Anne-Gaëlle Saint-Guirons

INRIA

INSTITUT NATIONAL DE RECHERCHE EN INFORMATIQUE ET EN AUTOMATIQUE

Construction and performance analysis of local *DtN absorbing boundary conditions for exterior Helmholtz problems. Part II : Prolate spheroid boundaries*

Hélène Barucq — Rabia Djellouli — Anne-Gaëlle Saint-Guirons

N° 6395

October 2007

Thème NUM

ISSN 0249-6399 ISRN INRIA/RR--6395--FR+ENG

INRIA
FUTURS

Construction and performance analysis of *local* DtN absorbing boundary conditions for exterior Helmholtz problems. Part II : Prolate spheroid boundaries

Hélène Barucq [*] , Rabia Djellouli[†] , Anne-Gaëlle Saint-Guirons[*]

Thème NUM — Systèmes numériques
Projet Magique 3D

Rapport de recherche n° 6395 — October 2007 — 31 pages

Abstract: We propose a new class of approximate *local* DtN boundary conditions to be applied on prolate spheroid-shaped exterior boundaries when solving acoustic scattering problems by elongated obstacles. These conditions are : (a) exact for the first modes, (b) easy to implement and to parallelize, (c) compatible with the local structure of the computational finite element scheme, and (d) applicable to exterior elliptical-shaped boundaries that are more suitable in terms of cost-effectiveness for surrounding elongated scatterers. Moreover, these conditions coincide with the classical local DtN condition designed for spherical-shaped boundaries. We investigate analytically and numerically the effect of the frequency regime and the slenderness of the boundary on the accuracy of these conditions when applied for solving radiators and scattering problems. We also compare their performance to the second order absorbing boundary condition (BGT2) designed by Bayliss, Gunzburger and Turkel when expressed in prolate spheroidal coordinates. The analysis reveals that, in the low frequency regime, the new second order DtN condition (DtN2) retains a good level of accuracy *regardless* of the slenderness of the boundary. In addition, the DtN2 boundary condition outperforms the BGT2 condition. Such superiority is clearly noticeable for large eccentricity values.

Key-words: Absorbing boundary conditions, prolate spheroidal coordinates, Dirichlet-to-Neumann operator, scattering problems

[*] Laboratoire de Mathématiques Appliquées, CNRS UMR 5142, Université de Pau et des Pays de l'Adour, IPRA-Avenue de l'Université, 64013 Pau, France
[†] Department of Mathematics, California State University Northridge, CA 91330-8313, USA

Unité de recherche INRIA Futurs
Parc Club Orsay Université, ZAC des Vignes,
4, rue Jacques Monod, 91893 ORSAY Cedex (France)
Téléphone : +33 1 72 92 59 00 — Télécopie : +33 1 60 19 66 08

Construction et analyse de performance de conditions aux limites absorbantes de type DtN localisé pour des problèmes extérieurs d'Helmholtz. Partie II : Frontières sphéroïdales prolates

Résumé : Nous proposons une nouvelle classe de conditions aux limites absorbantes de type DtN localisé applicables à des frontières extérieures de forme ellipsoïdale lors de la résolution de problèmes de scattering d'ondes acoustiques par des obstacles allongés. Ces conditions sont : (a) exactes pour les premiers modes, (b) faciles à implémenter et à paralléliser, (c) compatibles avec la structure locale d'un schéma numérique de type éléments finis, et (d) applicables à des frontières extérieures de forme ellipsoïdale ce qui est plus approprié en terme de coût de calcul lorsque l'on entoure un obstacle allongé. De plus, ces conditions coïncident avec la condition DtN localisée classique construite pour des frontières de forme sphérique. Nous étudions analytiquement et au travers de tests numériques l'effet du régime de fréquence et de l'allongement de la frontière sur la performance de ces conditions lors de la résolution des problèmes de radiateur et de scattering. Nous comparons aussi leurs performances à celles de la condition aux limites absorbante d'ordre deux (BGT2) construite par Bayliss, Gunzburger et Turkel lorsqu'elle est exprimée en coordonnées sphéroïdales prolates. Cette analyse révèle que, en régime basse fréquence, la condition d'ordre deux DtN (DtN2) admet un très bon niveau de performance *quel que soit* l'allongement de la frontière. De plus, la condition aux limites DtN2 est plus performante que la condition BGT2. Cette supériorité apparaît clairement pour de grandes excentricités.

Mots-clés : Conditions aux limites absorbantes, coordonées sphéroïdales prolates, opérateur Dirichlet-to-Neumann, problèmes de scattering

1 Introduction

Exterior Helmholtz problems are classical mathematical models for studying scattering problems arising in many applications such as sonar, radar, geophysical exploration, nondestructive testing, etc... Despite their simplicity, this class of problems is not completely solved particularly from a numerical point of view. For example, the computation of the solutions of these problems requires first to limit it to a finite domain. This is often achieved by surrounding the given scatterer(s) (or radiator) by an artificial boundary that is located at some distance (measured in multiples of wavelength of interest) from its surface. A so-called "nonreflecting" boundary condition is then prescribed on the artificial boundary to represent the "far-field" behavior of the scattered field. The challenge here is the development of a simple but reliable as well as cost-effective computational procedure for representing the far-field behavior of the scattered. The quest for such conditions is ongoing (see, e.g., the recent review by Turkel in the book [18]).

We propose in this work new three-dimensional approximate *local* DtN boundary conditions to be employed on prolate spheroid boundaries that are primary candidates for surrounding elongated scatterers. The idea for constructing such conditions is driven by several considerations chief among them the following two reasons. First, the widely-used second order absorbing boundary condition (BGT2) designed by Bayliss, Gunzburger and Turkel for spherical-shaped boundaries [3] performs poorly when it is expressed in elliptical coordinates and applied to prolate spheroid boundaries in the low frequency regime [14]. The accuracy deteriorates significantly for large eccentricity values of the boundaries as observed in [14]. The damping effect introduced to this condition [15] improves the performance for small eccentricity values. However, the modified BGT2 still performs poorly for eccentricity values larger than 0.6 in the (relatively) low frequency regime (see Figure 15 in [15]). Hence, there is a need for constructing local absorbing boundary conditions (ABC) that extend the range of satisfactory performance. Second, the three-dimensional approximate local DtN conditions designed for spherical-shaped boundaries [10] perform very well for low wavenumber values as reported in [11]. We recall that, in $\mathbb{R}^3$, the second-order DtN boundary condition and the BGT2 condition are identical [11]. Nevertheless, using these conditions on spherical-shaped exterior boundaries when solving scattering problems by elongated scatterer often leads to larger than needed computational domains, which hampers computational efficiency. This suggests that approximate local DtN boundary conditions designed for prolate spheroidal-shaped boundaries is an attractive alternative for improving the computational performance.

Given that, this work is devoted to the construction of theses conditions and to the assessment of their performance when employed on prolate spheroidal-shaped boundaries for solving three-dimensional radiator and scattering problems. The idea of constructing three-dimensional approximate *local* DtN boundary conditions is not new. Indeed, as stated earlier, such conditions have been already derived for spherical-shaped boundaries [10]. The construction procedure adopted in [10] is based on the localization of the truncated global DtN boundary condition [12]. The key ingredient of this procedure is the trigonometric identities that express high order derivatives of sine and cosine functions. However, this

property is not satisfied by the angular spheroidal wave functions [4]. Consequently, the procedure used in [10] is no longer applicable to the truncated global DtN boundary operator when expressed in elliptical coordinates [8, 7]. Hence, the construction methodology we propose for deriving the class of approximate local DtN boundary conditions in prolate spheroidal coordinates can be viewed as an *inverse-type* approach. More specifically, we start from a Robin-type boundary condition with unknown coefficients. Unlike the case of polar coordinates, these coefficients depend on the angles (φ, θ) of the prolate spheroidal coordinates. Such dependence is necessary to preserve the symmetry and local nature of the resulting boundary conditions. Then, we require that the considered condition to be an exact representation of the first modes. Consequently, the coefficients are the unique solution of a linear algebraic system.

We assess mathematically and numerically the performance of the constructed approximate local DtN boundary conditions. More specifically, we analyze the effect of low wavenumber and the eccentricity on the performance of these conditions in the case of three-dimensional radiator and scattering problems. We adopt the on-surface radiation condition formulation (OSRC) [13] in order to perform *analytically* this investigation. We note that such formulation is *not* appropriate for high frequency regime as observed previously in [2]. The main interest in the following analyses is to evaluate the performance of the proposed approximate local DtN conditions at low wavenumber to see if relatively small computational domains can be employed in order to avoid excessive computational cost. The OSRC formulation must be viewed as an extreme case while an exterior elliptical-shaped boundary surrounding an elongated scatterer would be less "demanding" on the boundary condition. The analysis herein shows that, in the case of the radiator, we can observe the DtN2 condition performs similarly to the BGT2 condition for values of e smaller than 0.6 and it outperforms BGT2 when e is bigger than 0.6. In the case of the scattering problem, the DtN2 condition outperforms the BGT2 condition even for small values of e, the DtN2 solution being clearly better for $e \geq 0.6$.

The reminder of this paper is as follows. We specify in Section 2 the nomenclature and assumptions adopted in this paper. Then, we present the class of new local DtN boundary conditions in prolate spheroidal coordinates in Section 3, along with their properties. We show that these conditions are exact for the first modes. In section 4, we perform the mathematical and numerical analysis to assess computational performance of these conditions when applied for solving radiator and scattering problems. We conclude this work in Section 5.

2 Preliminaries

Throughout this paper, we use the prolate spheroidal coordinates (ξ, φ, θ) which are lrelated to the cartesian coordinates (x, y, z) by the following transformation:

$$x = b \sin\varphi \cos\theta,\ y = b \sin\varphi \sin\theta,\ z = a \cos\varphi \tag{1}$$

where $\varphi \in [0, \pi)$, $\theta \in [0, 2\pi)$. The parameters a and b respectively represent the major and the minor axes and are given by:

$$a = f \cosh \xi, \; b = f \sinh \xi \tag{2}$$

where ξ is a strictly positive real number and f is the interfocal distance and is defined by:

$$f = \sqrt{a^2 - b^2} \tag{3}$$

We also define the eccentricity e on a prolate spheroid at $\xi = \xi_0$, by:

$$e = \frac{1}{\cosh \xi_0} = \sqrt{1 - \frac{b^2}{a^2}} \tag{4}$$

The eccentricity e characterizes the slenderness of the surface. It satisfies $0 < e < 1$. Note that when $e \to 0$, the prolate spheroid degenerates into a sphere and when $e \to 1$, the spheroid degenerates into a line with length $2f$ on the z-axis.

We recall that the mn-th prolate spheroidal mode u_{mn} $(m \leq n)$ is given by [17]:

$$u_{mn} = R^{(3)}_{mn}(kf, \cosh \xi) S_{mn}(kf, \cos \varphi) \cos m\theta \tag{5}$$

The functions $R^{(3)}_{mn}(kf, \cosh \xi)$ are the radial spheroidal wave functions of the third kind and $S_{mn}(kf, \cos \varphi)$ denote the angular spheroidal wave functions which are solution to the differential equation [4]:

$$\frac{\partial}{\partial \varphi} \left(\sin \varphi \frac{\partial S_{mn}}{\partial \varphi} \right) + \sin \varphi \left(\lambda_{mn} - (kf)^2 \cos^2 \varphi - \frac{m^2}{\sin^2 \varphi} \right) S_{mn}(kf, \cos \varphi) = 0 \tag{6}$$

where $\lambda_{mn} := \lambda_{mn}(kf)$ is called the prolate spheroidal eigenvalue (see p.11 in Ref. [4]).

3 The new approximate *local* boundary conditions and their derivation

Next, we construct the new local DtN absorbing boundary conditions in prolate spheroidal coordinates, and describe their properties.

3.1 The approximate local DtN boundary conditions in Prolate spheroidal coordinates

The three-dimensional first- (DtN1) and second-order (DtN2) local Dirichlet-to-Neumann boundary conditions, defined on the prolate spheroid-shaped surface $\xi = \xi_0$, are given by:

$$\text{DtN1}: \quad \frac{\partial u}{\partial \xi} = \frac{\sqrt{1-e^2}}{e} R_{00}\, u \tag{7}$$

$$\text{DtN2}: \quad \frac{\partial u}{\partial \xi} = \frac{\sqrt{1-e^2}}{(\lambda_{01}-\lambda_{00})\, e} \left[\left(\lambda_{01} R_{01} - \lambda_{00} R_{00} - (R_{00} - R_{01}) \left(eka\right)^2 \cos^2 \varphi \right) u + (R_{00} - R_{01})\, \Delta_\Gamma u \right] \tag{8}$$

where the coefficients R_{mn} depend on the radial spheroidal wave functions of the third kind $R_{mn}^{(3)}$, the wavenumber ka, and the eccentricity e as follows:

$$R_{mn} = \frac{\dfrac{\partial R_{mn}^{(3)}}{\partial \xi}(eka, e^{-1})}{R_{mn}^{(3)}(eka, e^{-1})} \tag{9}$$

and Δ_Γ denotes the Laplace Beltrami operator, which reads in prolate spheroidal coordinates (ξ, φ, θ) as:

$$\Delta_\Gamma = \frac{1}{\sin\varphi} \frac{\partial}{\partial \varphi} \left(\sin\varphi \frac{\partial}{\partial \varphi} \right) + \frac{1}{\sin^2 \varphi} \frac{\partial^2}{\partial \theta^2} \tag{10}$$

The following four remarks are noteworthy:

- First, the Robin-type boundary condition (7) (resp. (8)) is, by construction, an exact representation of the first (resp. the first and second) prolate spheroidal mode(s) (see Eq.5).
- Second, the boundary conditions (7), (8) are called *local* DtN conditions because they result from a localization process of the truncated global DtN boundary operator defined in [8, 7]. The local feature of these conditions is of a great interest from a numerical view point. Indeed, the incorporation of these conditions in any finite element code introduces only mass- and stiffness-type matrices defined on the exterior boundary. The coefficients λ_{mn} and R_{mn} can be computed once for all at the preprocessing level.
- Third, it must be point out that when $e = 0$ (the prolate spheroid becomes a sphere), conditions (7) and (8) are identical to the three-dimensional DtN conditions designed for spherical shaped boundaries [10, 11]. This property can be easily established using the asymptotic behavior of the radial spheroidal wave functions of the third kind $R_{mn}^{(3)}$ and the prolate spheroidal eigenvalues λ_{mn}.
- Last, approximate local DtN conditions of order higher than two are inappropriate for conventional finite element implementations since they require regularity higher than C^0. Consequently, we consider only the first (DtN1) and second order (DtN2) conditions in the following.

3.2 The procedure for constructing the approximate local DtN conditions

As stated earlier in the introduction, the idea of constructing approximate *local* DtN boundary conditions is not new. Indeed, such conditions have been already derived for spherical-shaped boundaries in [10]. The construction procedure adopted in [10] is based on the localization of the truncated global DtN boundary condition [7]. The key ingredient of this procedure is the trigonometric identities that express high order derivatives of sine and cosine functions (see for example Eqs. (C15-C21) p. 215 in [9] for the 3D case). However, this property is not satisfied by the angular spheroidal wave functions (see Eq. (6)), and therefore, the procedure used in [10] cannot be applied to the truncated global DtN boundary operator when expressed in elliptical coordinates [8, 7]. The approach we propose for constructing these approximate local DtN boundary condition in the case of prolate spheroid-shaped boundaries can be viewed as an *inverse-type* methodology. More specifically, we start from a Robin-type boundary condition with unknown coefficients. These coefficients depend on the prolate spheroidal eigenvalue.In addition, we require that the considered condition is an exact representation of the first modes. Consequently, the coefficients are the unique solution of a linear algebraic system. Next, we describe this procedure for construction the approximate local DtN1 and DtN2 conditions given by (7) and (8).

i. *Construction of the first order DtN1 boundary condition*

We consider a Robin-type boundary condition that is an exact representation of the first spheroidal mode u_{00} given by Eq. (5). Hence, we set:

$$\frac{\partial u}{\partial \xi} = Au \tag{11}$$

where the constant A satisfies

$$(\sinh\xi)\,\frac{\partial R^{(3)}_{mn}}{\partial \xi}(kf,\cosh\xi)S_{00}(kf,\cos\varphi) = A\left(R^{(3)}_{00}(kf,\cosh\xi)S_{00}(kf,\cos\varphi)\right) \tag{12}$$

Then, we substitute, at $\xi=\xi_0$, Eqs, (2)-(4) into Eq. (12), and deduce that

$$A = \frac{\sqrt{1-e^2}}{e}\,R_{00} \tag{13}$$

where R_{00} is given by Eq. (9).

ii. *Construction of the second order DtN2 boundary condition*

The goal here is to construct a Robin-type boundary condition that is an exact representation of the first two modes u_{00} and u_{01} given by Eq. (5). Hence, we set::

$$\frac{\partial u}{\partial \xi} = C\,u + D\,(\Delta_\Gamma - (eka)^2\cos^2\varphi)u \tag{14}$$

where C and D are constant (independent of φ) to be determined. Note that, unlike DtN2 boundary condition for the spherical-shaped boundaries, the coefficients of this condition depend on the angular variable φ. Such dependence is necessary for constructing a *symmetric* boundary condition since the angular spheroidal wave functions satisfied differential equation given by Eq. (6). Indeed, it is easy to verify that, for all modes u_{mn}, we have:

$$\Delta_\Gamma u_{mn} = \left(-\lambda_{mn} + (eka)^2\cos^2\varphi\right) u_{mn} \tag{15}$$

In order to determine the constants C and D, we assume that, at $\xi = \xi_0$, we have:

$$\frac{\partial u_{mn}}{\partial \xi} = C\,u_{mn} + D\,\left(\Delta_\Gamma - (eka)^2\cos^2\varphi\right) u_{mn}\;; \quad m = 0 \quad \text{and} \quad n = 0, 1 \tag{16}$$

Then, using Eq. (15), it follows that (C, D) is the unique solution of the folllowing 2×2 linear system:

$$\begin{cases} C - D\,\lambda_{00} &= \dfrac{\sqrt{1-e^2}}{e}\,R_{00} \\ \\ C - D\,\lambda_{01} &= \dfrac{\sqrt{1-e^2}}{e}\,R_{01} \end{cases} \tag{17}$$

where the coefficients R_{mn} are given by Eq. (9).
The DtN2 boundary condition given by Eq. (8) is a direct consequence of solving the system (17) and substituting the expressions of (C, D) into Eq. (14).

4 The performance of the new approximate local DtN conditions

In the following, we assess analytically and numerically the performance of the approximate local DtN1 and 2 boundary conditions given by (7) and (8). More specifically, we analyze the effect of low wavenumber ka and the eccentricity e on the performance of DtN1 and DtN2 in the case of both radiator and scattering problems. We adopt the on-surface radiation condition formulation (OSRC) [13] in order to perform this investigation analytically. We note that such formulation is not appropriate for high frequency regime as observed previously in [2]. The main interest in the following analyses is to evaluate the performance of the proposed approximate local DtN conditions at low ka to see if relatively small computational domains can be employed in order to avoid excessive computational cost. The

OSRC formulation is an extreme case while an exterior elliptical-shaped artificial boundary surrounding an elongated scatterer would be less "demanding" on the boundary condition. As in [11, 14, 15], we assess the performance of the ABCs DtN1 and DtN2 using the *specific impedance* introduced in [5, 6] as a practical tool for measuring the efficiency of ABCs in the context of the OSRC formulation. This *non-dimensional* quantity measures the effect of the truncated medium in physical terms. It provides a convenient indicator of the performance of a given approximate representation. In the elliptical coordinates system, the specific impedance can be expressed as follows:

$$Z = \frac{i\sqrt{1-e^2}\, ka\, u}{\dfrac{\partial u}{\partial \xi}}\,|_{\xi=\xi_0} \tag{18}$$

4.1 The performance of the local DtN conditions for single prolate spheroidal mode

Next, we assess analytically and numerically the performance of the approximate local DtN1 and DtN2 boundary conditions given by (7) and (8) when applied to three-dimensional radiator problems. Recall (see Eq. (64), p. 3645 in [14]), that the exact specific impedance $Z^{\rm ex3}_{mn}$, for the mn-th prolate spheroidal mode, on the surface of a prolate spheroid at $\xi = \xi_0$ is given by:

$$Z^{\rm ex3}_{mn} \;=\; \frac{{\rm i}\sqrt{1-e^2}kaR^{(3)}_{mn}(eka,e^{-1})}{\dfrac{\partial R^{(3)}_{mn}}{\partial \xi}(eka,e^{-1})} \;=\; \frac{{\rm i}eka}{R_{mn}} \tag{19}$$

where the coefficient R_{mn} is given by Eq. (9). In addition, Its asymptotic behavior as $ka \to 0$ (see Eq. (67), p. 3646 n [14]) is given by:

$$Z^{\rm ex3}_{mn} \sim \left(\frac{(ka)^{n+1}}{(n+1)(2n-1)!!}\right)^2 - {\rm i}\frac{ka}{n+1}; \quad \text{as} \quad ka \to 0 \tag{20}$$

where the double factorial is defined in [11, 1].

4.1.1 Analytical study

The following lemma states the expression of the approximate specific impedances for the mn-th prolate spheroidal mode, on the surface of a prolate spheroid at $\xi = \xi_0$. This lemma results from substituting $u = u_{mn}$ in Eq. (18), and using the boundary conditions (7) and (8) to evaluate $\dfrac{\partial u_{mn}}{\partial \xi}$ (see [16] for the detailed proof).

Lemma 4.1 *The approximate specific impedance ($Z^{\rm DtN1}_{mn}$) corresponding to the first-order Dirichlet-to-Neumann absorbing boundary condition (DtN1) is given by:*

$$Z^{\rm DtN1}_{mn} = Z^{\rm ex3}_{00} \tag{21}$$

The approximate specific impedance (Z_{mn}^{DtN2}) corresponding to the second-order Dirichlet-to-Neumann absorbing boundary condition (DtN2) is given by:

$$Z_{mn}^{\mathrm{DtN2}} = \frac{\lambda_{01} - \lambda_{00}}{(\lambda_{01} - \lambda_{mn}) \dfrac{1}{Z_{00}^{\mathrm{ex3}}} + (\lambda_{mn} - \lambda_{00}) \dfrac{1}{Z_{01}^{\mathrm{ex3}}}} \tag{22}$$

where $\lambda_{mn} := \lambda_{mn}(kf)$ is called the prolate spheroidal eigenvalue (see p.11 in Ref. [4]).

Remark 4.2 Note that when $e = 0$, that is the prolate spheroid degenerates to sphere, the approximate DtN specific impedances given by Eqs. (21) and (22) are identical to the ones obtained in the case of spherical-shaped radiators [11]. In addition, when $m = n = 0$ (resp. $(m, n) = (0, 1)$), Z_{mn}^{DtN2} coincides with Z_{00}^{ex3} (resp. with Z_{01}^{ex3}), as expected.

The next proposition states the asymptotic behavior of the approximate specific impedance Z_{mn}^{DtN2} as $ka \to 0$.

Proposition 4.3 *The asymptotic behavior of the DtN2 specific impedance of the mn^{th} ($m \leq n$) prolate spheroidal mode as $ka \to 0$ is given by:*

$$Z_{mn}^{\mathrm{DtN2}} \sim -2\frac{n(n+1)-2}{(n(n+1)+2)^2}(ka)^2 - \mathrm{i}\frac{2ka}{n(n+1)+2}; \quad n \geq 2 \tag{23}$$

Proof of Proposition 4.3. The asymptotic behavior of the DtN2 specific impedance given by Eq. (23) results from substituting the asymptotic behavior of the exact specific impedance given by Eq. (20) into Eq. (22) and from using the following property of the prolate spheroidal eigenvalues (see p.11 in Ref. [4]):

$$\lambda_{mn}(0) = n(n+1) \tag{24}$$

Remark 4.4 First, we note that the asymptotic behavior of Z_{mn}^{DtN1} (resp. Z_{mn}^{DtN2} ; $n \leq 1$) is identical to the behavior of the exact specific impedance Z_{00}^{ex3} (resp. Z_{mn}^{ex3} ; $n \leq 1$), which follows from the design of the DtN boundary conditions. Second, for $n \geq 2$, the asymptotic behavior for DtN2 is independent of the eccentricity e, and is identical to the case of a sphere (see Eq. (92), p. 32 in [11]) as well as to the approximate specific impedance corresponding to the second-order BGT condition when applied on prolate spheroid radiator (see Eq. (69), p. 3646 in [14]). Last, the asymptotic behavior given by Eq. (20) and Eq. (23) indicates that for higher modes ($n \geq 2$), the real part of the exact impedance tends to zero, as $ka \to 0$, faster than the DtN2 specific impedance. This result suggests that DtN2 boundary condition may not be appropriate for single higher modes.

4.1.2 Numerical investigation

We have performed several experiments to investigate numerically the effect of the wavenumber and the slenderness of the boundary on the performance of the second-order DtN boundary condition DtN2 given by Eq. (8) when computing single radiating modes. We have

compared the results to the ones obtained with BGT2 conditions when applied on prolate spheroid boundaries (see Figs. (18) to (21) in [14]). We report in this section the results obtained when computing modes $(m, n) = (0, 2)$ and $(m, n) = (1, 1)$ for illustration. More numerical results can be found in [16]. Note that for lower modes, DtN2 is exact, and therefore outperforms the BGT2 absorbing boundary condition. The numerical results presented here have been obtained for two low wavenumber values $ka = 0.1$ (see Figs. (1), (2), (5), and (6)), and for $ka = 1$ (see Figs. (3), (4), (7), and (8)). Because of the dependence of the BGT2 specific impedance on $\varphi \in [0, \pi)$ (see Eq. (69) in [14]), we have reported the obtained results on the magnitude of the specific impedance in polar coordinates, and the relative errors as a function of φ. These results are obtained for three eccentricity values $e = 0.1$ (a prolate spheroid boundary very close to a sphere), $e = 0.6$ (a "regular" prolate spheroid boundary), and $e = 0.9$ (the prolate spheroid boundary is very elongated). As expected (see Eq. (20) and Proposition 4.3), DtN2 boundary condition performs overall poorly when computing higher modes regardless of the wavenumber and eccentricity values since the relative error is above 25% for most situations (see Figs (2), (6), (4), and (8)). Note that the level of accuracy delivered by DtN2 boundary condition seems to be better than by BGT2 boundary condition (except for $e = 0.6$ when computing mode $(m, n) = (0, 2)$), yet this level of accuracy remains very high for practitioners. Last, when the prolate spheroid tends to be close to a sphere $e = 0.1$, both conditions retain an acceptable level of accuracy (the relative errors are less than 10%).

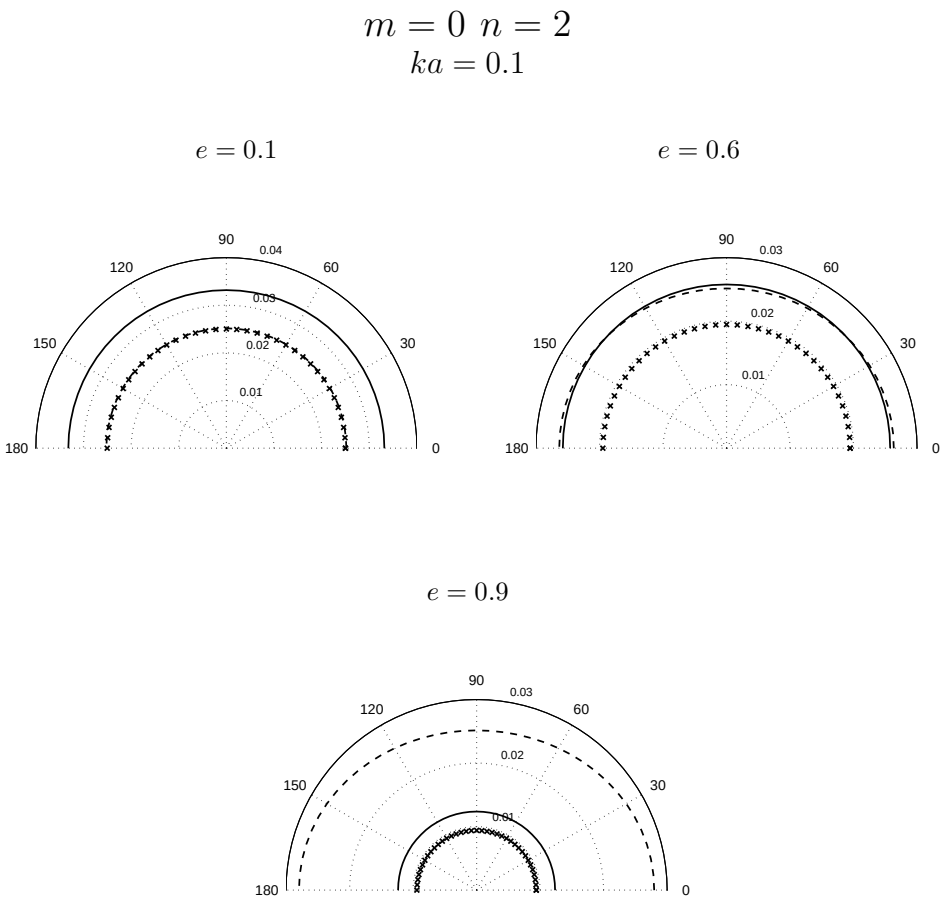

Figure 1: Absolute value of the specific impedance for the exact (solid), the DtN2 (crossed), the BGT2 (dashed).

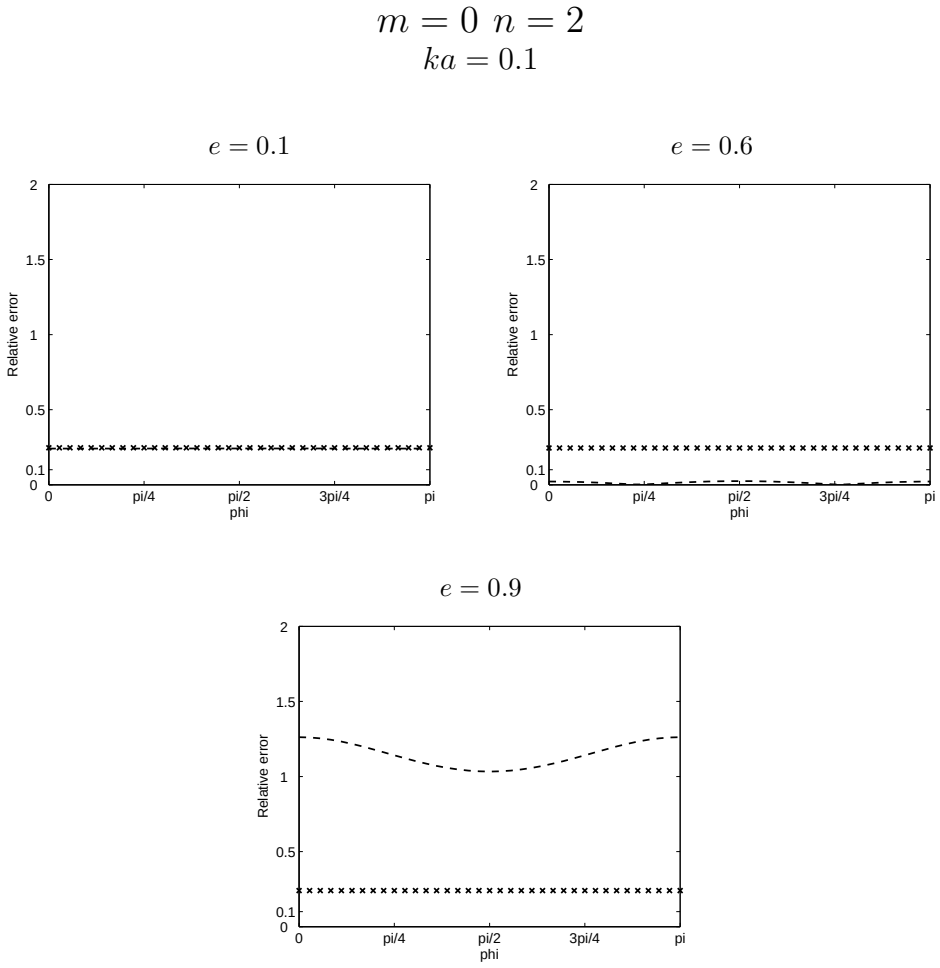

Figure 2: Relative error of the specific impedance for the DtN2 (crossed), the BGT2 (dashed).

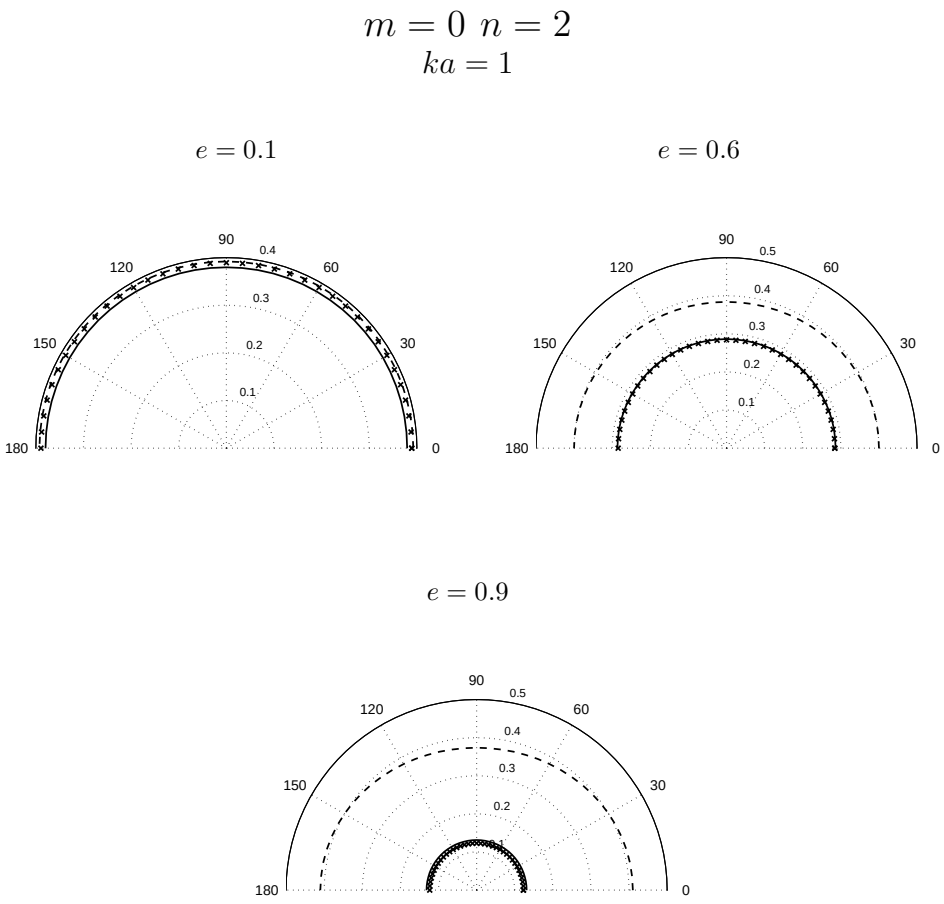

Figure 3: Absolute value of the specific impedance for the exact (solid), the DtN2 (crossed), the BGT2 (dashed).

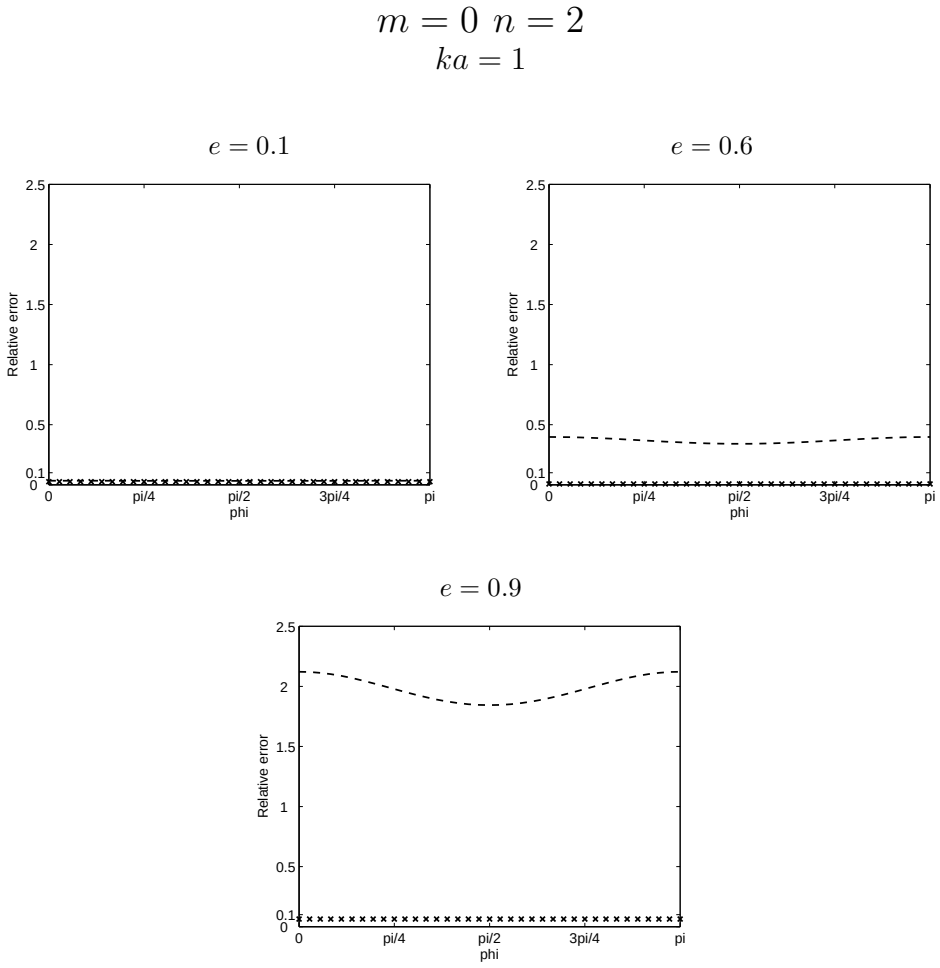

Figure 4: Relative error of the specific impedance for the DtN2 (crossed), the BGT2 (dashed).

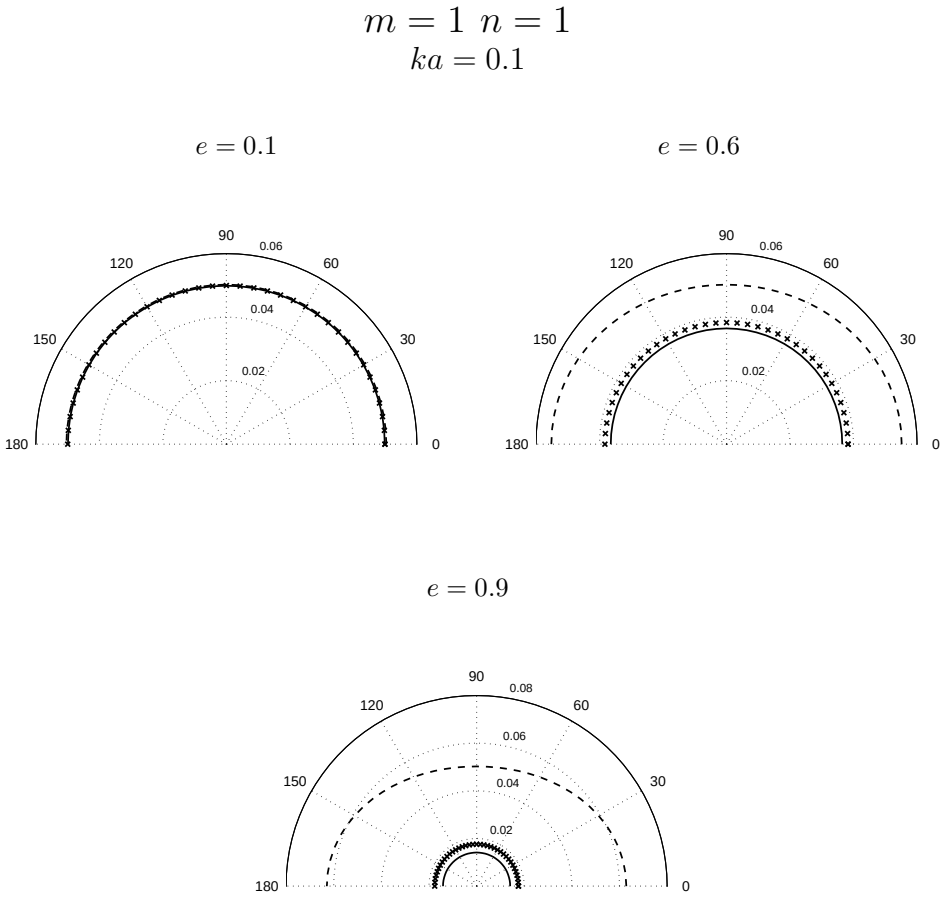

Figure 5: Absolute value of the specific impedance for the exact (solid), the DtN2 (crossed), the BGT2 (dashed).

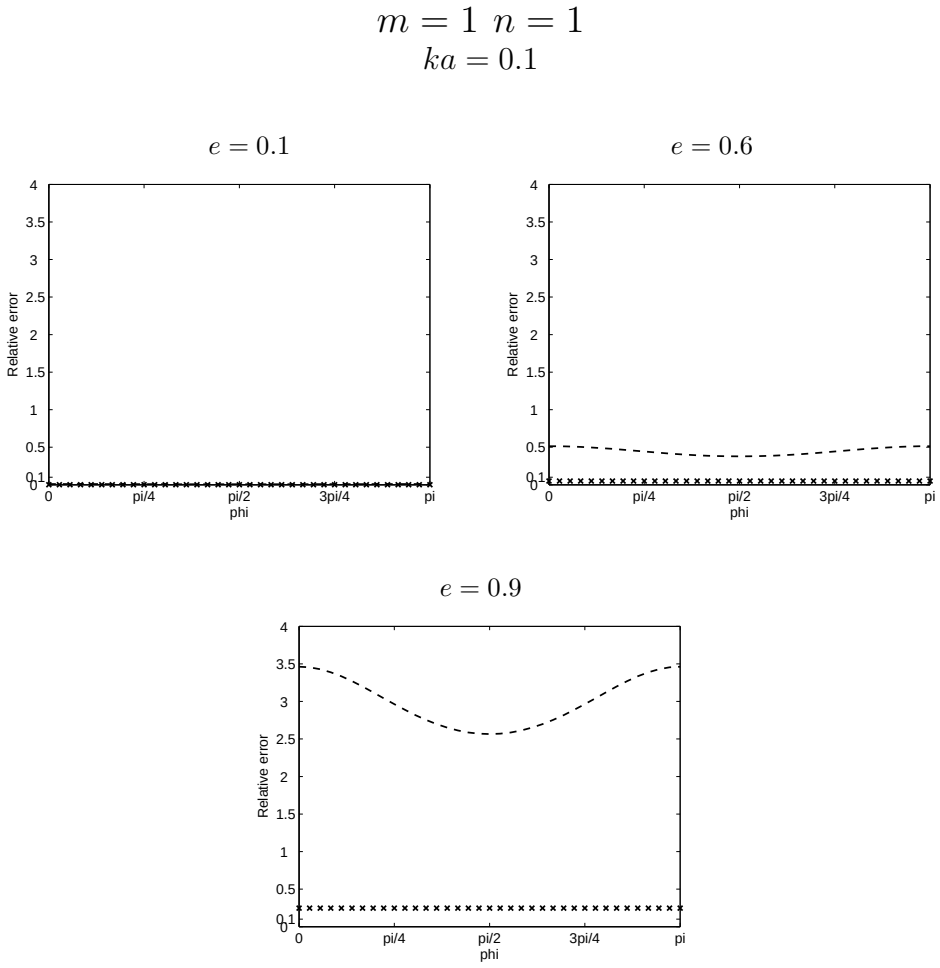

Figure 6: Relative error of the specific impedance for the DtN2 (crossed), the BGT2 (dashed).

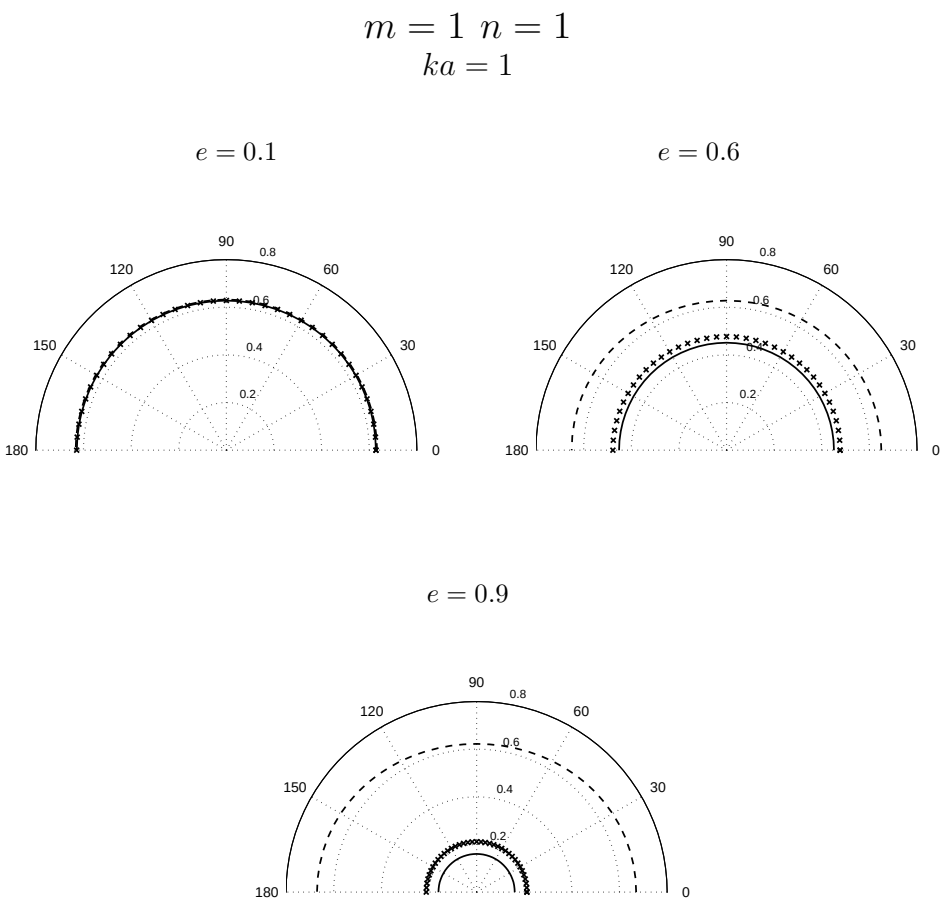

Figure 7: Absolute value of the specific impedance for the exact (solid), the DtN2 (crossed), the BGT2 (dashed).

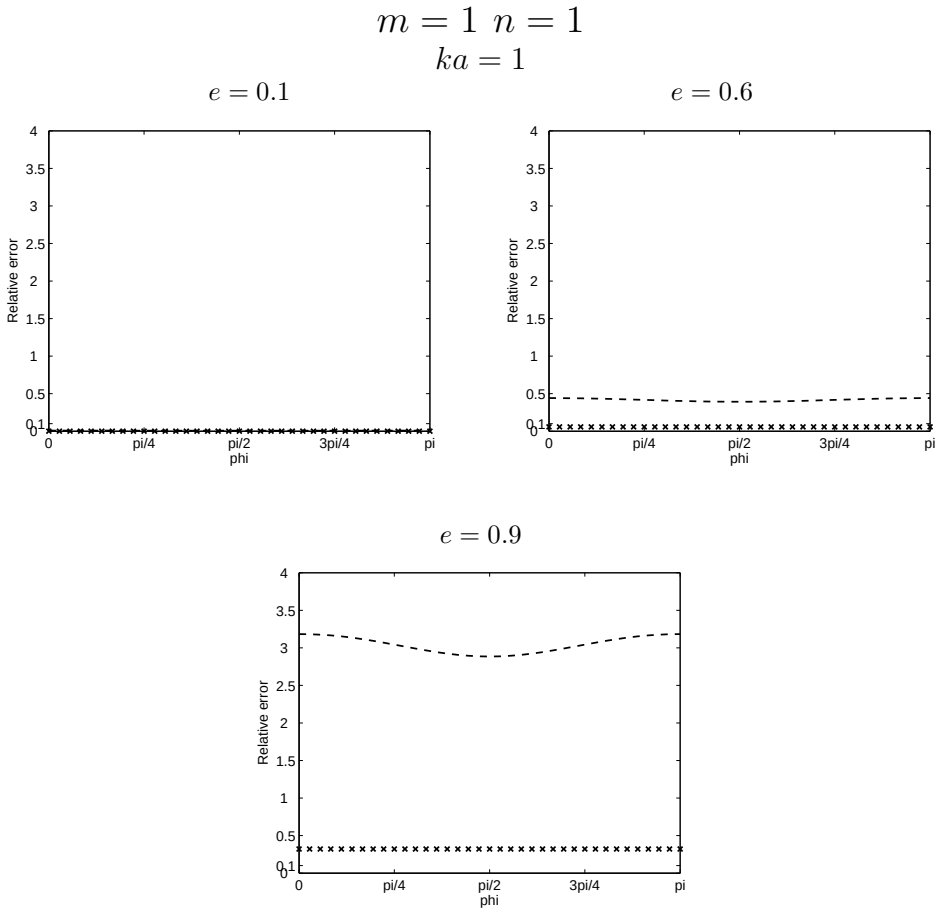

Figure 8: Relative error of the specific impedance for the DtN2 (crossed), the BGT2 (dashed).

4.2 The performance of the local DtN conditions for prolate spheroid-shaped scatterer

Next, we assess analytically and numerically the performance of the approximate local DtN1 and DtN2 boundary conditions given by (7) and (8) when applied to three-dimensional scattering problems by sound-soft prolate spheroid-shaped obstacle . Recall (see Eq. (85), p. 3649 in [14]), that the exact specific impedance Z^{ex3} on the surface of a prolate spheroid at $\xi = \xi_0$ is given by:

$$Z^{\text{ex3}} = -\frac{\mathrm{i}\sqrt{1-e^2}ka\, u^{\text{inc}}}{\dfrac{\partial}{\partial\xi}\,(u^{\text{scat}})|_{\xi=\xi_0}} \tag{25}$$

where u^{inc} is the incident plane wave with incident angle φ_0 defined by

$$u^{\text{inc}} = \mathrm{e}^{\mathrm{i}kf\cosh\xi(\cos\varphi\cos\varphi_0+\tanh\xi\sin\varphi\sin\varphi_0\cos\theta)} \tag{26}$$

u^{scat} is the acoustic scattered field by a sound-soft prolate spheroid-shaped obstacle. u^{scat} can be represented by the following series [17]

$$u^{\text{scat}} = -2\sum_{m=0}^{\infty}\sum_{n=m}^{\infty}(2-\delta_{0m})A_{mn}\mathrm{i}^n R^{(3)}_{mn}(kf,\cosh\xi)S_{mn}(kf,\cos\phi)\cos m\theta \tag{27}$$

where

$$A_{mn} = \frac{R^{(1)}_{mn}(eka,e^{-1})S_{mn}(eka,\cos\phi_0)}{N_{mn}R^{(3)}_{mn}(eka,e^{-1})} \tag{28}$$

and N_{mn} represents the normalization factor of the angular spheroidal wave functions [4] and δ_{0m} is the Kronecker delta symbol.
Moreover, we also recall (see Eq. (91), p. 3655 in [14]), that the asymptotic behavior of the exact specific impedance Z^{ex3} of the scattered field on the surface of a prolate spheroid as $ka \to 0$ is given by:

$$Z^{\text{ex3}} \sim Z^{\text{ex3}}_{00} \sim (ka)^2 - \mathrm{i}ka \tag{29}$$

where Z^{ex3}_{00} is given by Eq. (20) for $m = n = 0$.

4.2.1 Analytical study

The next lemma states the expression of the approximate specific impedances on the surface $\xi = \xi_0$ of a prolate spheroid sound-soft scatterer. This lemma results from substituting $u = -u^{\text{inc}}$ in Eq. (18), and using the boundary conditions (7) and (8), and the expression of the incident plane wave given by Eq. (26) to evaluate $\dfrac{\partial u^{\text{inc}}}{\partial\xi}$ at $\xi = \xi_0$ (see [16] for the detailed proof).

Lemma 4.5 *The approximate specific impedance (Z^{DtN1}) corresponding to the first-order Dirichlet-to-Neumann boundary condition (DtN1) is given by:*

$$Z^{\mathrm{DtN1}} = Z_{00}^{\mathrm{ex3}} \tag{30}$$

The approximate specific impedance (Z^{DtN2}) corresponding to the second-order Dirichlet-to-Neumann boundary condition (DtN2) is given by:

$$Z^{\mathrm{DtN2}} = \frac{\lambda_{01} - \lambda_{00}}{\left(\dfrac{\lambda_{01}}{Z_{00}^{\mathrm{ex3}}} - \dfrac{\lambda_{00}}{Z_{01}^{\mathrm{ex3}}}\right)\left(-2i\alpha ka - (ka)^2\,\delta - (eka)^2\cos\varphi\right)} \tag{31}$$

where

$$\alpha = \cos\varphi\cos\varphi_0 + \sqrt{1-e^2}\sin\varphi\sin\varphi_0\cos\theta, \quad \delta = \left(\frac{\partial\alpha}{\partial\varphi}\right)^2 + \frac{1}{\sin^2\varphi}\left(\frac{\partial\alpha}{\partial\theta}\right)^2 \tag{32}$$

Remark 4.6 Note that when $e = 0$, that is the prolate spheroid degenerates to sphere, the approximate DtN specific impedances given by Eqs. (21) and (22) are identical to the ones obtained in the case of spherical-shaped scatterers [11].

The next proposition states the asymptotic behavior of the second-order DtN approximate specific impedance Z^{DtN2} as $ka \to 0$.

Proposition 4.7 *The asymptotic behavior of the approximate specific impedance Z^{DtN2} as $ka \to 0$ is given by:*

$$Z^{\mathrm{DtN2}} \sim (1-\alpha)\,(ka)^2 - \mathrm{i}ka \tag{33}$$

Proof of Proposition 4.7. The asymptotic behavior of the DtN2 specific impedance given by Eq. (33) results from substituting the asymptotic behavior of the exact specific impedance given by Eq. (20) into Eq. (31) and from using the the property of the prolate spheroidal eigenvalues given by Eq. (24).

Remark 4.8 First, we note that the asymptotic behavior of Z^{DtN1} is identical to the behavior of the exact specific impedance Z^{ex3} (see Eq. (29) and Eq. (30)). Second, Eq. (33) indicates that the asymptotic behavior of Z^{DtN2} depends on the eccentricity as well as on the observation angle φ. This dependence is comparable to the asymptotic behavior of the BGT2 approximate specific impedance (see Eq. (93), p. 3657 in [14]). Last, when $e = 0$, the asymptotic of both Z^{DtN1} and Z^{DtN2} are identical to the case of spheres (see Eq. (140) p. 47 in [11]).

4.2.2 Numerical investigation

We have performed several experiments to investigate numerically the effect of the wavenumber and the slenderness of the boundary on the performance of the second-order DtN boundary condition DtN2 given by Eq. (8) when solving sound-soft scattering problems in the OSRC context. We have compared the results to the ones obtained with BGT2 conditions

when applied on prolate spheroid boundaries (see Figs. (22) to (33) in [14]). We report in here the results obtained for three different values of the incidence angle $\varphi_0 = 0, \frac{\pi}{4}$ and $\frac{\pi}{2}$ for illustration. More numerical results can be found in [16]. Moreover, since the impedences in this case depend on $\varphi \in [0, \pi)$ and $\theta \in [0, 2\pi)$, we have reported 3D plots of obtained results in Figs. (9)-(14). These results have been obtained for three eccentricity values $e = 0.1$ corresponding to a prolate spheroid boundary very close to a sphere (see Fig. (9) and Fig. (12)), $e = 0.6$ corresponding to a "regular" prolate spheroid boundary (see Fig. (10) and Fig. (13)), and $e = 0.9$ (corresponding to a very elongated prolate spheroid boundary (see Fig. (11) and Fig. (14)). One can observe that unlike the radiator problem, the DtN2 boundary condition delivers an excellent level of accuracy in the low frequency regime for all eccentricity values. Indeed, the results depicted in Figs. (12), (13), and (14) indicate that the relative error on the approximate DtN2 specific impedance is always below 2%, while The BGT2 accuracy deteriorates significantly for $e \geq 0.6$ (the relative error is larger than 40%).

$$e = 0.1$$

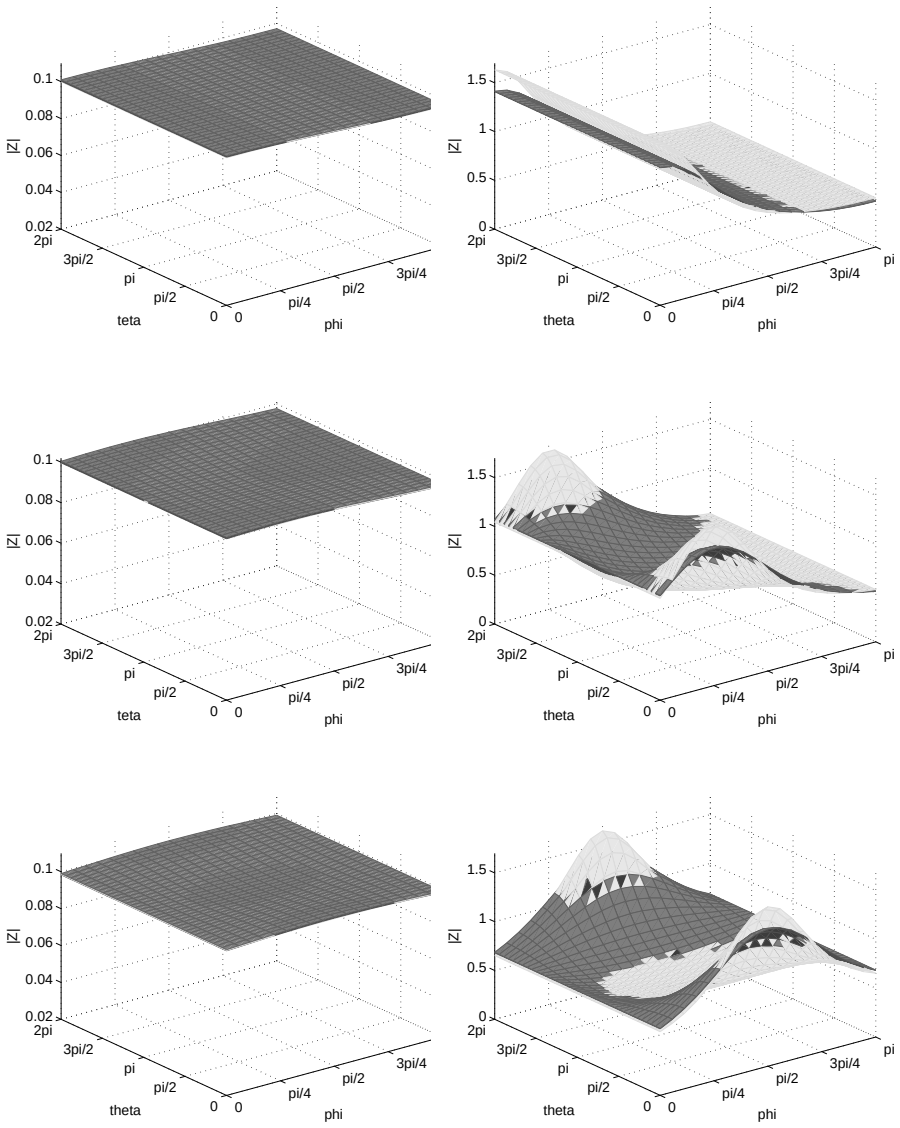

Figure 9: Absolute value of the specific impedance for the exact (clear grey), the DtN2 (black), the BGT2 (dark grey) for $ka = 0.1$ (left) and $ka = 1$ (right) for the incident angles $\theta_0 = 0$ (up), $\theta_0 = \frac{\pi}{4}$ (middle), $\theta_0 = \frac{\pi}{2}$ (down).

$e = 0.6$

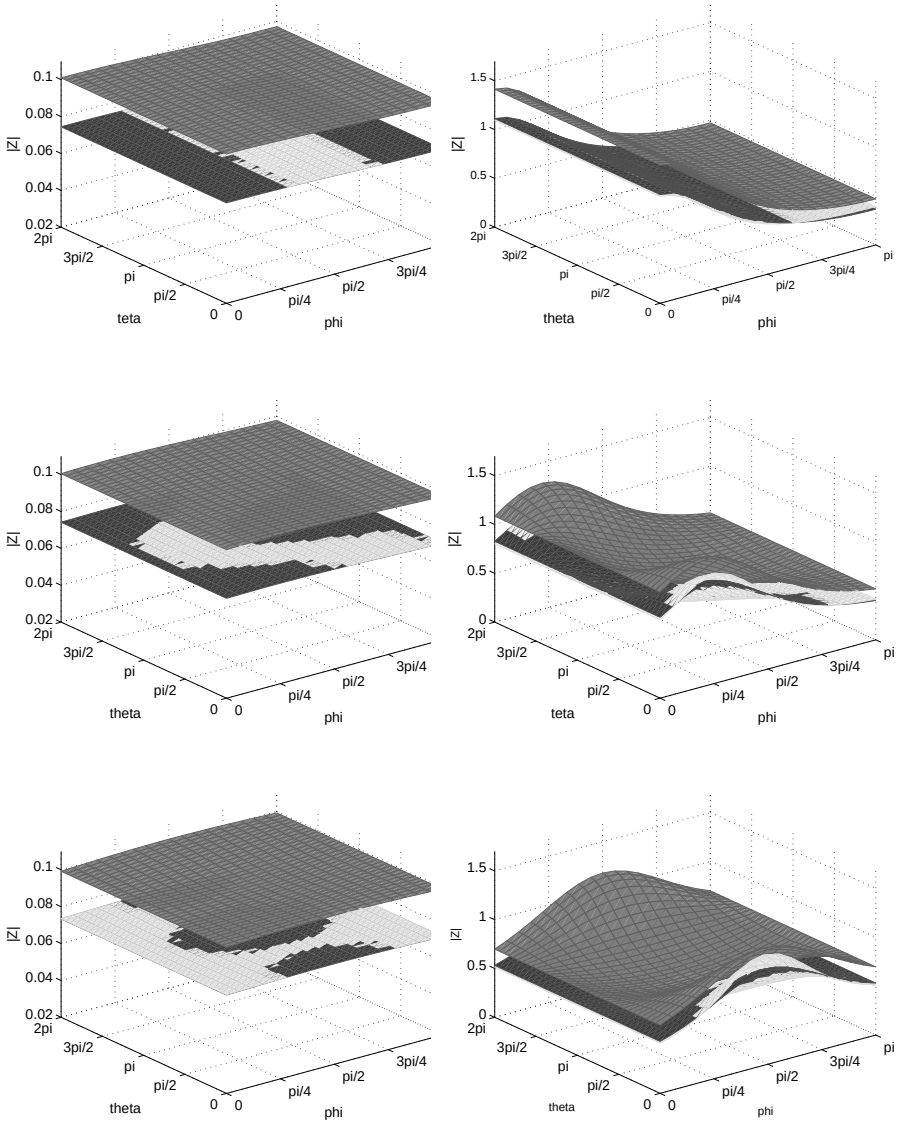

Figure 10: Absolute value of the specific impedance for the exact (clear grey), the DtN2 (black), the BGT2 (dark grey) for $ka = 0.1$ (left) and $ka = 1$ (right) for the incident angles $\theta_0 = 0$ (up), $\theta_0 = \frac{\pi}{4}$ (middle), $\theta_0 = \frac{\pi}{2}$ (down).

$e = 0.9$

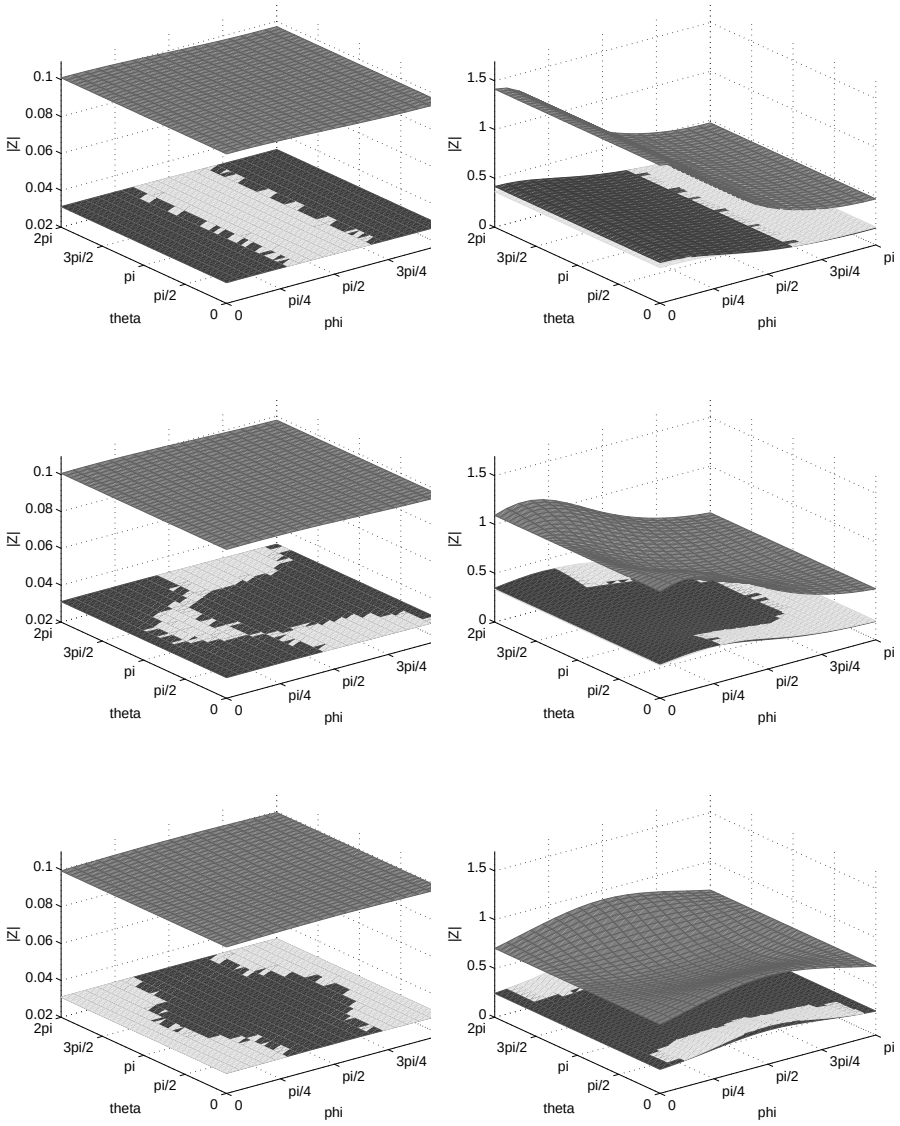

Figure 11: Absolute value of the specific impedance for the exact (clear grey), the DtN2 (black), the BGT2 (dark grey) for $ka = 0.1$ (left) and $ka = 1$ (right) for the incident angles $\theta_0 = 0$ (up), $\theta_0 = \frac{\pi}{4}$ (middle), $\theta_0 = \frac{\pi}{2}$ (down).

$e = 0.1$

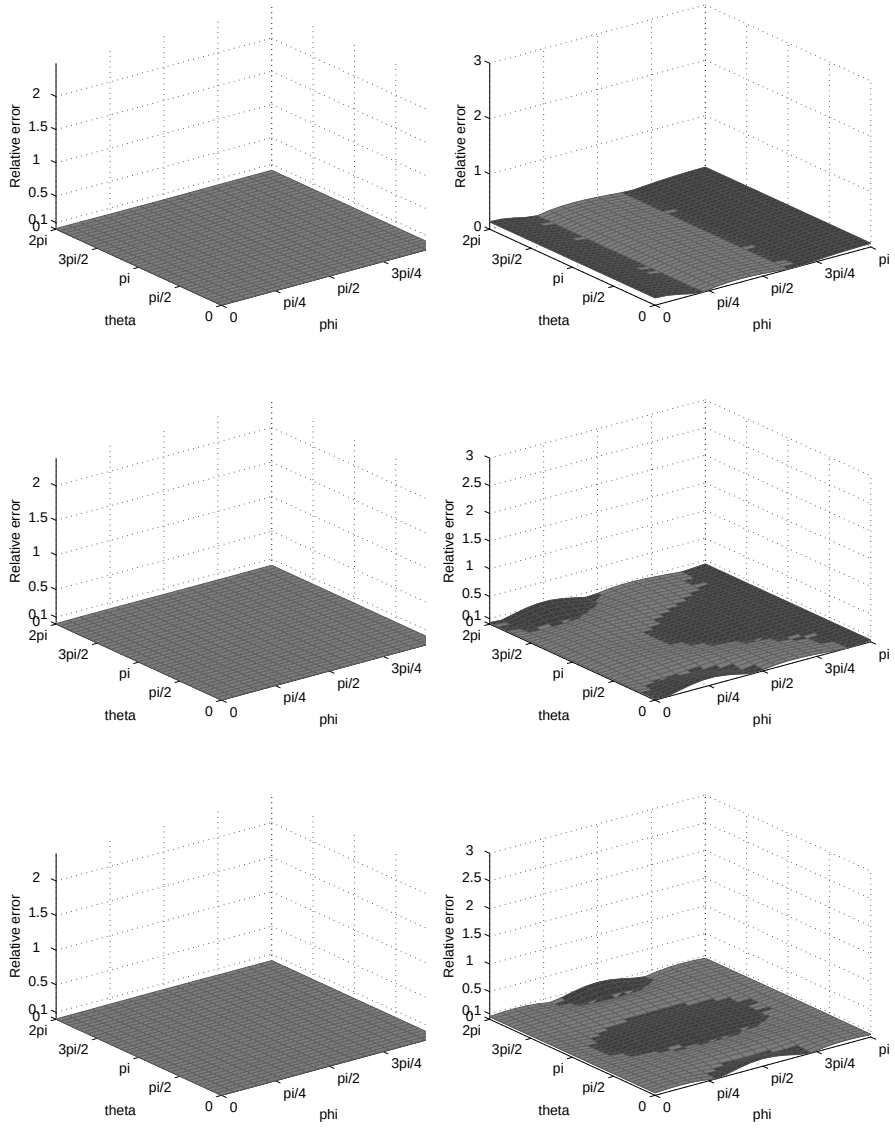

Figure 12: Relative error of the specific impedance for the DtN2 (black), the BGT2 (dark grey) for $ka = 0.1$ (left) and $ka = 1$ (right) for the incident angles $\theta_0 = 0$ (up), $\theta_0 = \frac{\pi}{4}$ (middle), $\theta_0 = \frac{\pi}{2}$ (down).

$e = 0.6$

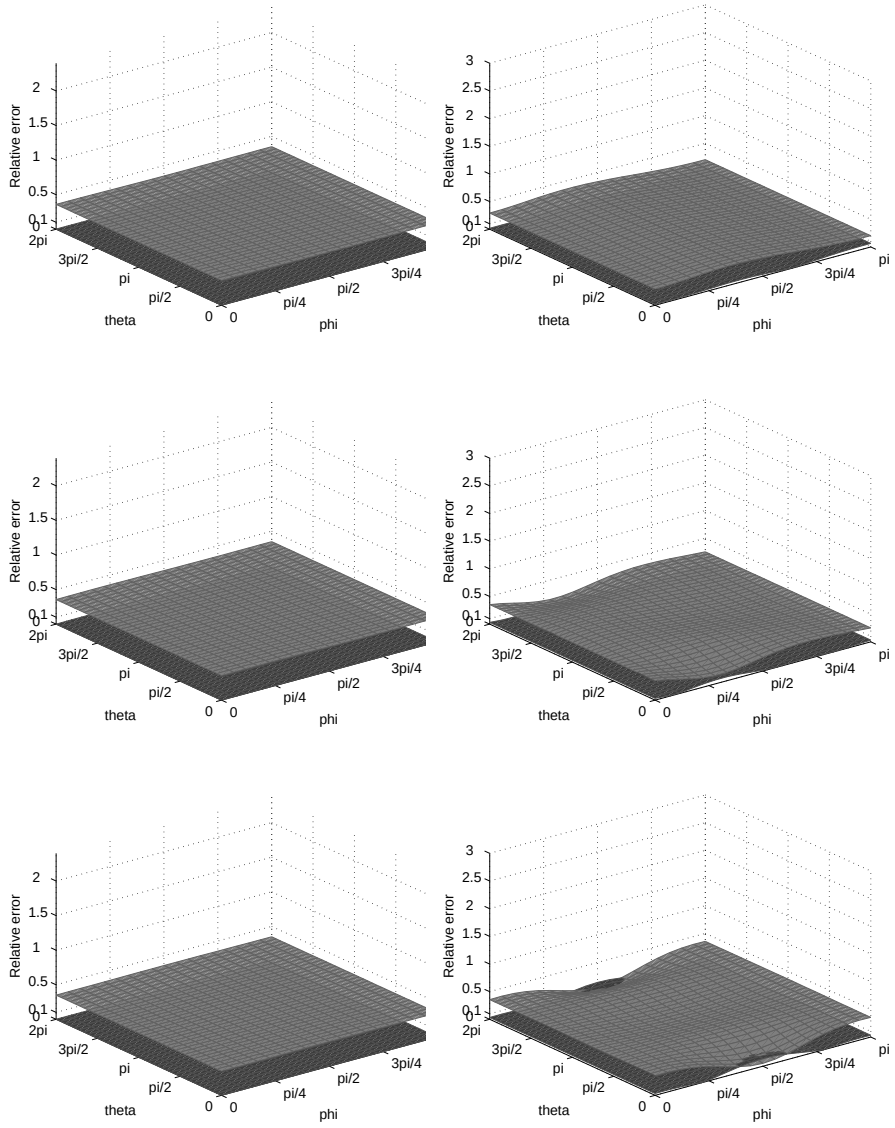

Figure 13: Relative error of the specific impedance for the DtN2 (black), the BGT2 (dark grey) for $ka = 0.1$ (left) and $ka = 1$ (right) for the incident angles $\theta_0 = 0$ (up), $\theta_0 = \frac{\pi}{4}$ (middle), $\theta_0 = \frac{\pi}{2}$ (down).

$$e = 0.9$$

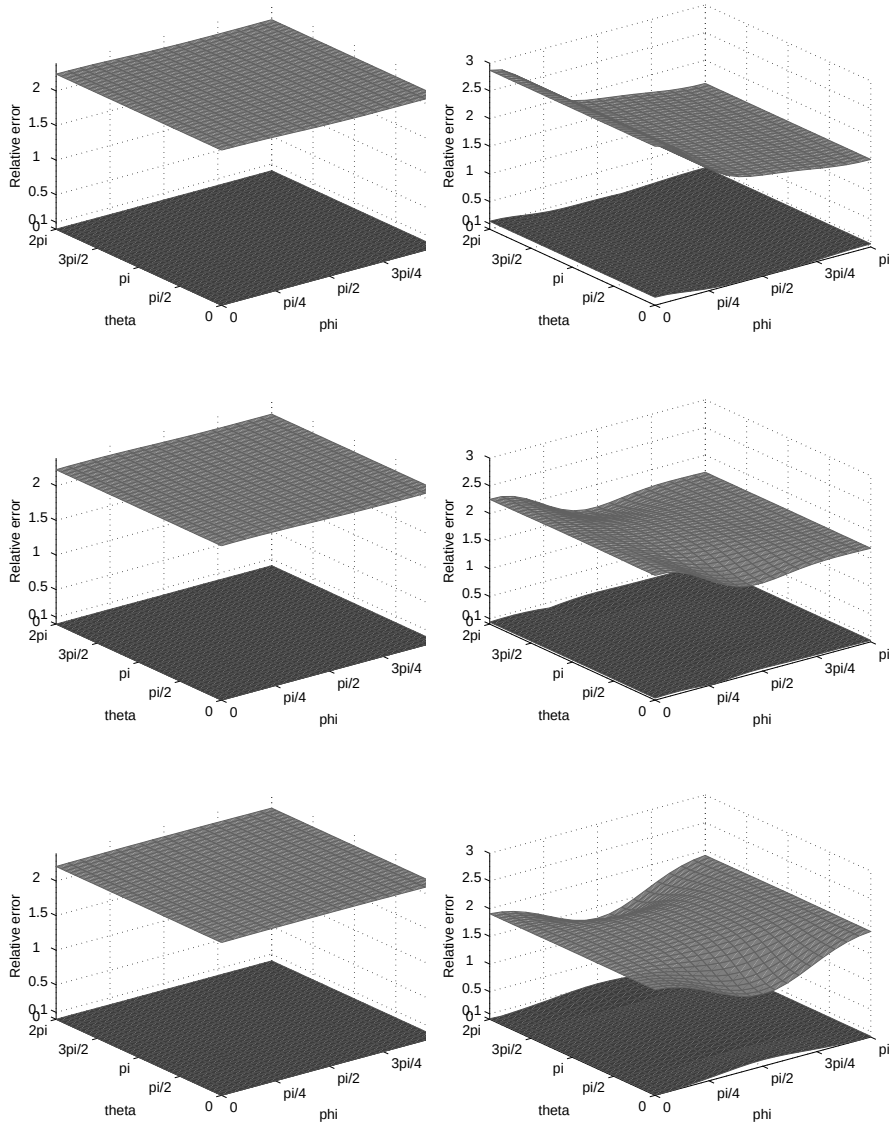

Figure 14: Relative error of the specific impedance for the DtN2 (black), the BGT2 (dark grey) for $ka = 0.1$ (left) and $ka = 1$ (right) for the incident angles $\theta_0 = 0$ (up), $\theta_0 = \frac{\pi}{4}$ (middle), $\theta_0 = \frac{\pi}{2}$ (down).

5 Conclusion

We have designed a new class of approximate local ABCs to be applied on elliptical-shaped exterior boundaries when solving acoustic scattering problems by elongated obstacles. These conditions are *exact* for the first radiation modes, they are easy to implement and to parallelize, and they preserve the local structure of the computational finite element scheme. The analysis reveals that in the case of the radiator, DtN2 boundary conditions, by construction, outperforms the BGT2 conditions while performing similarly for small values of e and the DtN2 boundary condition outperforms BGT2 for lower single modes. However, for higher modes both conditions performs poorly. In the case of the scattering problem, the situation is different. Indeed, the BGT2 boundary conditions performs poorly for eccentricity values $e \geq 0.6$, while the DtN2 boundary condition delivers an excellent level of accuracy in the low frequency regime for all eccentricity values. We plan to investigate the effect of large values of the wavenumber on the accuracy of the DtN2 condition.

Acknowledgements

The authors acknowledge the support by INRIA/CSUN Associate Team Program. Any opinions, findings, conclusions or recommendations expressed in this material are those of the authors and do not necessarily reflect the views of INRIA or CSUN.

References

[1] M. Abramovitz, I. Stegun, Handbook of Mathematical Functions with Formulas, Graphs and Mathematical Tables, Dover Publications, New York, 1972

[2] X. Antoine, Fast approximate computation of a time-harmonic scattered field using the on-surface radiation condition method, IMA J. Appl. Math., 66(1):83–110, 2001

[3] A. Bayliss, M. Gunzberger, and E. Turkel, Boundary conditions for the numerical solution of elliptic equations in exterior regions, SIAM J. Appl. Math., 42 (2), pp. 430-451, 1982

[4] C. Flammer, Spheroidal Functions, Standford University Press, Standford, CA, 1957

[5] T. L. Geers, Doubly asymptotic approximations for transient motions of submerged structures, J. Acoust. Soc. Am., 64 (5), pp. 1500-1508, 1978

[6] T. L. Geers, Third-order doubly asymptotic approximations for computational acoustics, J. Comput. Acoust., 8 (1), pp. 101-120, 2000

[7] D. Givoli, Exact representations on artificial interfaces and applications in mechanics, AMR, 52(11):333–349, 1999

[8] M. J. Grote, J. B. Keller, On nonreflecting boundary conditions, J. Comput. Phys., 122, 2, 231-243, 1995

[9] I. Harari, Computational methods for Problems of Acoustics with Particular Reference to Exterior Domains, PhD thesis, Stanford university, May 1991

[10] I. Harari and T. J. R. Hughes, Analysis of continuous formulations underlying the computation of time-harmonic acoustics in exterior domains, Comput. Methods Appl. Mech. Engrg., 97(1):103–124, 1992

[11] I. Harari, R. Djellouli, Analytical study of the effect of wave number on the performance of local absorbing boundary conditions for acoustic scattering, Applied Numerical Mathematics, 50, 15-47, 2004

[12] J. B. Keller, D. Givoli, Exact nonreflecting boundary conditions, J. Comput. Phys., 82 (1), 172-192,1989

[13] G. A. Kriegsmann, A. Taflove, and K. R. Umashankar, A new formulation of electromagnetic wave scattering using an on-surface radiation boundarycondition approach, IEEE Trans. Antennas and Propagation 35 (2), 153–161, 1987

[14] R.C. Reiner, R. Djellouli, and I. Harari, The performance of local absorbing boundary conditions for acoustic scattering from elliptical shapes, Comput. Methods Appl. Mech. Engrg, 195, 3622-3665, 2006

[15] R.C. Reiner and R. Djellouli, Improvement of the performance of the BGT2 condition for low frequency acoustic scattering problems, Journal of Wave Motion, 43, pp. 406-424, 2006.

[16] A. Saint-Guirons, Construction et analyse de conditions aux limites absorbantes pour des problèmes de propagation d'ondes, Ph.D. thesis, (In Preparation).

[17] T. B. A. Senior, Scalar diffraction by a prolate spheroid at low frequencies, Canad. J. Phys. 38 (7) (1960) 1632-1641

[18] E. Turkel, Iterative methods for the exterior Helmholtz equation including absorbing boundary, conditions, In: Computational Methods for Acoustics Problems, F. Magoulès (ed.), Saxe-Coburg Publications (To Appear)

Contents

Unité de recherche INRIA Futurs
Parc Club Orsay Université - ZAC des Vignes
4, rue Jacques Monod - 91893 ORSAY Cedex (France)

Unité de recherche INRIA Lorraine : LORIA, Technopôle de Nancy-Brabois - Campus scientifique
615, rue du Jardin Botanique - BP 101 - 54602 Villers-lès-Nancy Cedex (France)
Unité de recherche INRIA Rennes : IRISA, Campus universitaire de Beaulieu - 35042 Rennes Cedex (France)
Unité de recherche INRIA Rhône-Alpes : 655, avenue de l'Europe - 38334 Montbonnot Saint-Ismier (France)
Unité de recherche INRIA Rocquencourt : Domaine de Voluceau - Rocquencourt - BP 105 - 78153 Le Chesnay Cedex (France)
Unité de recherche INRIA Sophia Antipolis : 2004, route des Lucioles - BP 93 - 06902 Sophia Antipolis Cedex (France)

Éditeur
INRIA - Domaine de Voluceau - Rocquencourt, BP 105 - 78153 Le Chesnay Cedex (France)
http://www.inria.fr
ISSN 0249-6399